

# ELECTRIC FIELD ENHANCEMENT FACTORS AROUND A METALLIC, END-CAPPED CYLINDER

S. PODENOK

*Department of Semiconductor Physics and Nano-Electronics  
Belarussian State University  
220050, Minsk, Belarus*

M. SVENINGSSON\*, K. HANSEN and E. E. B. CAMPBELL

*Department of Physics, Göteborg University  
SE-41296 Göteborg, Sweden*

*\*martin.sveningsson@chalmers.se*

Received 13 April 2006

Revised 14 June 2006

We have calculated the electric field enhancement factor for a metallic cylinder with a hemispherical end-cap in a plane capacitor geometry paying particular attention to the dependence of the field enhancement factor on the anode distance. In addition, we have investigated the angular dependence of the local field at the end-cap. The numerical results, which cover a range of different ratios of cylinder lengths and anode distances, can be fitted with simple functional expressions which provide a useful scaling for calculations of field emission currents from closed cap carbon nanotubes or nanowires.

*Keywords:* Electron field emission; field enhancement factor; carbon nanotubes; Fowler–Nordheim theory.

## 1. Introduction

Field emission involves the extraction of electrons from a solid by tunneling through a surface potential barrier in an external electric field. Fowler and Nordheim<sup>1</sup> derived an expression for the emission current density  $j$  that mainly depends on the work function of the material  $\phi$ , and the local electric field  $F_l$  at the surface of the emitter, apart from fundamental constants: In their equation, the current density  $j$ , depends on  $F_l$  as

$$j = \frac{q^3}{2\pi h} \cdot \frac{\sqrt{\mu}}{(\phi + \mu)\sqrt{\phi}} \cdot F_l^2 \exp\left(-\frac{4\kappa\phi^{3/2}}{3qF_l}\right), \quad (1)$$

where  $F_l$  is given in V/m and  $\mu$  is the Fermi energy.  $\kappa^2 = 8\pi^2 m/h^2$  ( $m$  is the mass of the electron),  $q$  is

the numerical value of the electron charge. The local electric field  $F_l$  appears in the denominator of the argument of the exponential and has a very strong influence on the magnitude of the emission current. Usually, this field is small as compared to the characteristic field given by  $6.83 \cdot 10^9$  [V/m]  $(\phi/[eV])^{3/2}$ , typically by an order of magnitude, and a precise knowledge of the field is therefore essential for quantitative applications of the formula. Other expressions have been derived which include effects such as the image charge,<sup>2</sup> but the importance of the magnitude of the local field persists in these later developments.

Electron emission currents start to be measurable at fields in the order of  $10^8$ – $10^9$  V/m. Such

\*Corresponding author.

high fields are most easily achieved in the vicinity of conducting objects with small radii of curvature which locally amplify the external electric field,<sup>3</sup> and this is one of the reasons carbon nanotubes with their high aspect ratios have attracted interest. The electric field in the vicinity of a conducting protrusion will be larger than the so-called macroscopic applied electrical field  $F_{\text{applied}}$  (in a planar capacitance geometry, the latter is the uniform electrical field that would exist between two smooth plates without any protrusions) by the field amplification (or enhancement) factor

$$\gamma = \frac{F_l}{F_{\text{applied}}}. \quad (2)$$

It is important to note that the macroscopic applied field is defined differently by different authors as they investigate the field enhancement. Miller,<sup>4</sup> Xu *et al.*,<sup>5</sup> Smith *et al.*<sup>6</sup> and Axelsson *et al.*<sup>7</sup> used, for example, the definition  $F_{\text{applied}} = V_0/D$  (see Fig. 1 for notation), which makes the system approach a plane capacitor model with a resulting field amplification value of 1 in the limit  $D \rightarrow 0$ . Others<sup>8–10</sup> used  $F_{\text{applied}} = V_0/d$ , which gives a  $\gamma$  that increases as  $D$  goes towards zero. The relation between the two different definitions is given by

$$\gamma' = \frac{\gamma}{1 + (L/D) + (R/D)}, \quad (3)$$

where  $\gamma'$  corresponds to  $F_{\text{applied}} = V_0/D$  and  $\gamma$  to  $F_{\text{applied}} = V_0/d$ . In this report, we use the definition

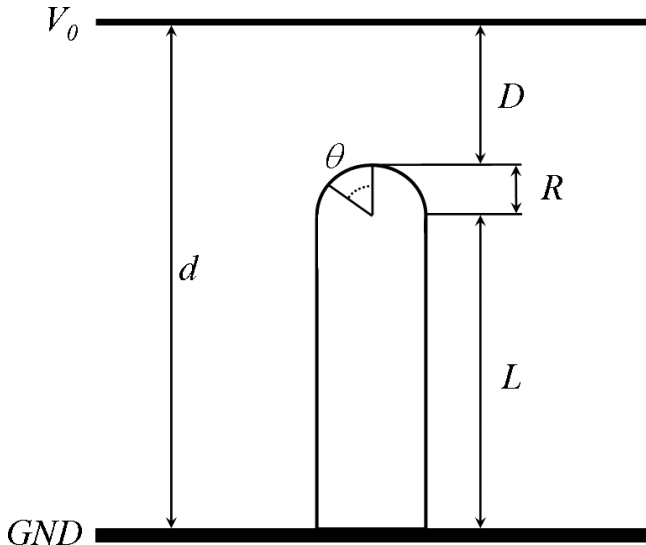


Fig. 1. Given geometry for a cylinder with an hemispherical end-cap.

$F_{\text{applied}} = V_0/d$ , which is the most widely used convention in the literature.

There exist a number of reports about calculations of  $\gamma$  for emitters like CNT (i.e., long conducting cylinders closed with a hemisphere).<sup>8,11,12</sup> Forbes *et al.*<sup>9</sup> made a critical review of these studies and found that all approximations to cylindrical emitters with shapes which are commensurate with analytically solvable models (e.g., floating sphere model, semi-ellipsoid on the plane) give poor results compared to the numerical simulations for the exact cylindrical surface. It is, however, clear from all these studies that  $\gamma$  has an almost linear dependence on  $L/R$ . Edgcombe and Valdre<sup>8</sup> gave the equation

$$\gamma = 1.2 \cdot \left( 3.15 + \frac{L}{R} \right)^{0.9}, \quad (4)$$

using the notation given in Fig. 1, while Miller<sup>4</sup> derived the formula (using the floating sphere model).

$$\gamma' = 3.5 + \frac{L}{R}. \quad (5)$$

Neither of these two cases gives any direct information on how  $\gamma$  depends on the separation between the emitter tip and the cathode,  $D$  (see Fig. 1 for notation) since the above mentioned formulas assume that  $D \gg L$ . The report by Miller includes a correction for the case when the dependence on  $D$  no longer can be neglected and gives an equation, which in our notation reads

$$\gamma' = \left( 3.5 + \frac{L}{R} \right) \cdot \frac{D}{d} + \exp \left( - \frac{D}{L+R} \cdot \left( 3.5 + \frac{L}{R} \right) \right), \quad (6)$$

where  $d = L + R + D$ . The situation when  $D$  is small or of the same order of magnitude as  $L$  has otherwise been awarded little attention in the literature. Wang *et al.*<sup>13</sup> continued the work by Miller on the floating sphere model and described the situation when the separation  $D$  is small as

$$\gamma = 3.5 + \frac{L}{R} + 1.202 \cdot \left( \frac{L}{L+D+R} \right)^3. \quad (7)$$

However, this formula does not give much difference in the results for small values of  $D$ . Instead the results imply that  $\gamma$  is increased by adding a factor, which is for all possible configurations, less than the given constant 1.202. This correction is small and

is not consistent with the results presented in this paper. Bonard *et al.*<sup>10</sup> gave another formula

$$\gamma = 1.2 \cdot \left( 3.15 + \frac{L}{R} \right)^{0.9} \times \left( 1 + 0.013 \frac{d}{D} - 0.033 \frac{D}{d} \right), \quad (8)$$

which has been fitted from data in a figure by Edgcombe and Valdre<sup>8</sup> that is strictly valid for  $L/R = 100$ . Bonard found that the predicted values overshoot the experimentally measured values by roughly a factor of two. As the authors also note, a comparison of experimental and theoretical values is fraught with uncertainties because of the lack of knowledge of the parameters entering the field emission formula, such as the work function,  $\phi$ , and screening from neighboring nanotubes that affects the local field.

Systematic studies of the effect of the anode location for CNTs were performed by Smith *et al.*,<sup>14</sup> but due to limitations of the software, the emitter was modeled as a parallelepiped closed by a semi-cylinder and these results are not directly applicable for calculations of the  $\gamma$  factors for CNTs. Axelsson *et al.*<sup>7</sup> calculated the change in the field enhancement factor for a specific field emission-based three-terminal relay where the nanotube is suspended horizontally above the anode and found that the value of  $\gamma$  depends on the anode distance.

Electron field emission from sharp emitter tips, such as carbon nanotubes, becomes more and more important when  $D \leq L$ . There are possible applications using field emission of electrons in nanoelectromechanical systems<sup>7</sup> or in the development of low energy consumption lamps,<sup>15,16</sup> ion gauges,<sup>17,18</sup> X-ray sources<sup>19</sup> and flat panel displays.<sup>20</sup> It is therefore very important to have a quantitative description of how the field enhancement factor is affected when the separation between the emitter tip and the anode is changed, since this will affect the tunneling current.

An important question that arises when we try to simulate the emission current from an hemispherical end-cap, with for example Eq. (1), is that the local field is not constant over the whole cap.<sup>21</sup> There is an angular distribution giving rise to a reduction of  $F_l$  as one moves towards the edge of the cap. It is therefore not correct to assume that the cap area of the conducting carbon nanotube is the true emission area. Effectively, the emission area

is reduced, with a reduction factor which depends on the applied field. We therefore also derive a simple expression for the angular variation of  $\gamma$  with the position on the end-cap.

This manuscript is devoted to the calculations of the field enhancement factor. In addition to the field enhancement factor, several other factors are needed to describe field emission. Questions relevant to field emission which will not be dealt with here include the issue of treating all electrodes as perfect conductors, the neglect of any effects arising from the quantum mechanical nature of the electron motion (“spill-out” from the surface), and the role of the image charge. The numerical solutions presented here for the local external electric field can be usefully combined with microscopic treatments of these questions.

## 2. Calculations

We solved numerically the Laplace equation in cylindrical coordinates with boundary conditions shown in Fig. 1 by the finite elements method<sup>22</sup> with an adaptive triangle mesh algorithm. The emitter was treated as an ideal conductor at the same constant potential (ground) as the cathode plate. The anode plate was treated as an ideal conductor biased at  $V = 1$  V. All dimensions are in length units of  $R$ . The boundary conditions at the outer cylinder diameter were chosen to correspond to a uniform electric field, i.e., the flux through the open boundary was set to zero. The boundary was placed at  $5d$  from the symmetry axis to minimize the fringe effects. Mesh refining was stopped and calculations treated as converged when the relative error between two subsequent numerical solutions for the potential was less than  $10^{-6}$  at every point of the mesh. The length of the sides of polygons adjacent to the tip in the apex region after final mesh refinement was  $2.5 \cdot 10^{-3}R$ .

After the converged potential was obtained, the  $\gamma$  factor was calculated as the ratio of the maximum electric field at the tip apex to the uniform field  $V_0/d$ .

The calculations were carried out as a function of the dimensionless ratios  $L/R$  and  $D/L$ , with  $L/R$  varying from 10 to 3000, and  $D/L$  from 0.01 to 10 in steps of a factor of 3 to obtain an approximately uniform range in a logarithmic scale for both of these quantities.

### 3. Fit of Numerical Data

The enhancement factor at the tip apex (i.e., the maximum value for a given geometry) was fitted independently of the angular dependence of the local field at the tip, and we describe these two fits separately.

The dominant component in the dependence of the enhancement factor on  $D/R$  and  $L/R$  is the dependence on  $L/R$ . We have therefore expressed the enhancement factor as

$$\gamma = f\left(\frac{L}{R}\right) \cdot g\left(\frac{L}{D}, \frac{D}{R}\right), \quad (9)$$

where  $f$  and  $g$  are functions to be determined. Initially, we leave  $f$  unspecified and optimize  $g$  for each value of  $L/R$ . We expect the enhancement factors to be independent of  $D$  in the limit of large  $D/R$ , because the field close to the anode should be fairly independent of  $D$  and  $L$  and equal to the average field,  $F \approx V_0/(D + L + R)$ , where  $V_0$  is the potential between anode and cathode. For small values of  $D/R$ , on the other hand, the field between the anode and the tip is approximately constant with a value of  $V_0/D$ , giving a field enhancement factor equal to  $(L + D + R)/D$ . These limits suggest that  $\gamma$  can be fitted with a Laurent series in  $D$ , with coefficients that may depend on  $L$ . We have found that the best fit with the somewhat arbitrary choice of three fit parameters is given by a form slightly different from a Laurent series, viz.

$$g = \left(1 + a_1 \frac{L}{D}\right) \times \left(1 + a_2 \frac{R}{D}\right) \cdot \left(1 + a_3 \left(\frac{R}{D}\right)^2\right), \quad (10)$$

with parameters:  $a_1 = 3.08 \cdot 10^{-3}$ ,  $a_2 = 0.818$  and  $a_3 = -9.18 \cdot 10^{-3}$ . This expression breaks down at very small values of  $D$ , around  $D \sim \sqrt{-a_3}R \approx 0.1R$  because the enhancement factor becomes negative. This is not a serious problem because it corresponds to an electrode-tube separation of typically one or a few tenths of a nanometer. At these separations, we expect the calculation to have marginal validity in any case because it is close to a length scale where neither the tube nor the surface can be treated as continuous, classical objects.

The optimal values of the parameters entering  $g$  were found by minimizing the root-mean-square deviation of the simulated points for each value of  $L/R$  separately. Division of  $\gamma$  with  $g$  then reduces the values to a single function of  $L/R$ . One point

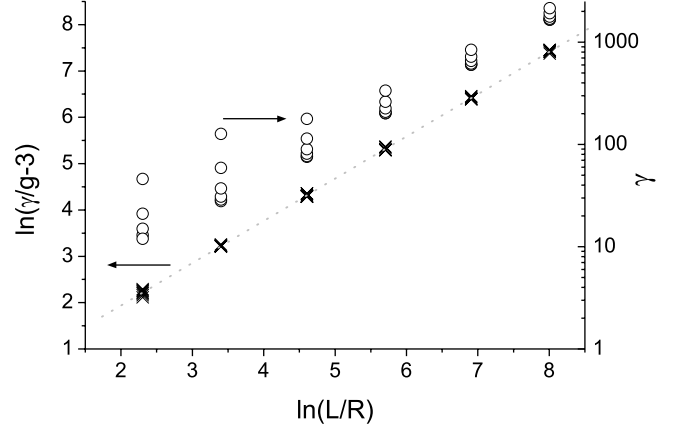


Fig. 2. The correction of the calculated  $\gamma$  values with the function  $g - 3$  gives a linear plot as a function of the natural logarithm of  $L/R$  (crosses). This indicates the accuracy of the function  $g$  and  $f$  in Eq. (10). The right hand axis corresponds to the original  $\gamma$  values, shown as circles. These data points show a large spread depending on the separation  $D$  for each  $L/R$  value.

on this curve is known from analytical calculations, that of  $L/R = 0$  (and  $D \rightarrow \infty$ ), corresponding to a hemispherical protrusion on a plate, for which  $\gamma = 3$  (see Refs. 9 and 23). In this limit,  $g = 1$ . Figure 2 shows the behavior of  $\gamma/g - 3$  versus  $L/R$ , in a double logarithmic plot. The function is very well represented by a straight line with a slope slightly below unity. The figure also shows the values of  $\gamma$  before division with  $g$ . The final functional form is

$$\gamma = \left(3 + 1.13 \left(\frac{L}{R}\right)^{0.912}\right) \cdot g\left(\frac{L}{D}, \frac{R}{D}\right), \quad (11)$$

where  $g$  is given by Eq. (10).

As an example of the resulting agreement, we show in Fig. 3 how  $\gamma$  depends on  $D$  for the tube length  $L/R = 30$  and  $L/R = 300$ , and give in addition a comparison between the model by Miller (Eq. (6)), Wang (Eq. (7)) and Bonard (Eq. (8)). The results by Edgcombe which are constant with  $D$  are also shown. Our calculated values are indicated with stars.

We observe that for large values of  $D$ , the prediction of  $\gamma$  converges towards the same value for models given by Edgcombe, Bonard and ours. There is a small offset for the other two models which has its origin in the exponential of  $L/R$ . However, there is a large difference for small values of  $D$  where some of the earlier literature formulae are

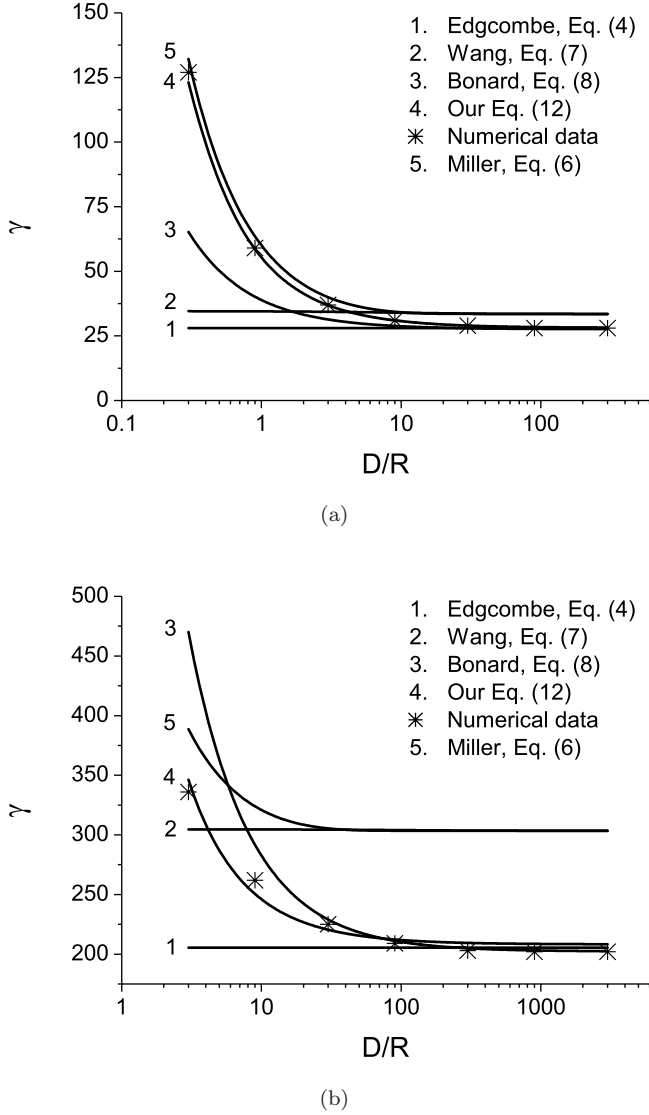


Fig. 3. Comparison of literature values of  $\gamma$  as a function of the separation  $D$  for (a)  $L/R = 30$  and (b)  $L/R = 300$ . The original data points are marked with stars.

in serious error. The model described by Bonard gives best agreement with our results, although this formula is, as mentioned before, extracted from calculations only valid for  $L/R = 100$ . For  $L/R = 300$ , Bonard's equation gives too high values for  $\gamma$ , for  $L/R = 30$ , too low values, and the agreement is good for  $L/R = 100$ . Hence, the results for the special case treated in Ref. 10 agree with those derived here for the same value of  $L/R$ . The values of  $\gamma$  calculated by Axelsson *et al.*,<sup>7</sup> are slightly lower than what Eq. (11) predicts. However, these calculations are only valid for the specified nanorelay geometry, which is different from ours. We unfortunately cannot compare Eq. (11) to the recent report by

Xu *et al.*<sup>5</sup> since important information about the carbon nanotube length is left out.

#### 4. Angular Dependence

The angular dependence of the field across the tip is important for the determination of the effective area from which field emission occurs. The angular dependence is less crucial than the maximum value for the integrated emission current because it will integrate out and enter as a pre-exponential factor only. It is nevertheless of some interest because it will introduce a field dependence on the pre-exponential, in addition to the one already stated in Eq. (1). From the simulations, we observe that the values can, to a good approximation, be expressed as

$$\frac{F_l(\theta)}{F_0} = 1 + h\left(\frac{L}{R}, \frac{D}{R}\right)\theta^2, \quad (12)$$

where  $\theta$  is the angle, in radians, from the top of the cap, indicated in Fig. 1 and  $F_0 = F_l(\theta = 0)$ . The function  $h$  is given by the specific geometry and has been analyzed similar to the functions  $f$  and  $g$  which describe  $\gamma(\theta = 0)$ . It can be parameterized as

$$h\left(\frac{L}{R}, \frac{D}{R}\right) = \left(c_0 + c_1 \frac{R}{L}\right) \times \left(1 + c_2 \frac{R}{D} + c_3 \left(\frac{R}{D}\right)^2\right), \quad (13)$$

with the parameter values:  $c_0 = -7.71 \cdot 10^{-2}$ ,  $c_1 = -0.659$ ,  $c_2 = 0.232$  and  $c_3 = 2.81$ . For large values of  $L/R$  and  $D/R$ , the angular dependence reduces to approximately  $F(\theta)/F_0 = 1 + c_0\theta^2$ . The use of this function in Eq. (12) gives a good description of how the local field changes over the endcap up to a value around 1 radian for the angle  $\theta$ . This is shown in Fig. 4 where the values of the local field, extracted from solving the Laplace equation, are compared with the full expression given by Eqs. (12) and (13). This point corresponds to around 85% of the local field at the apex of the end-cap. At larger angles and smaller fields, the emission current becomes exponentially suppressed and the angular dependence becomes less important. From the fits to the simulated data, we see that the deviations from a purely quadratic angular dependence render the emission current calculated with Eq. (12) slightly too high.

The effect of the angular dependence on the emission current can be calculated with an

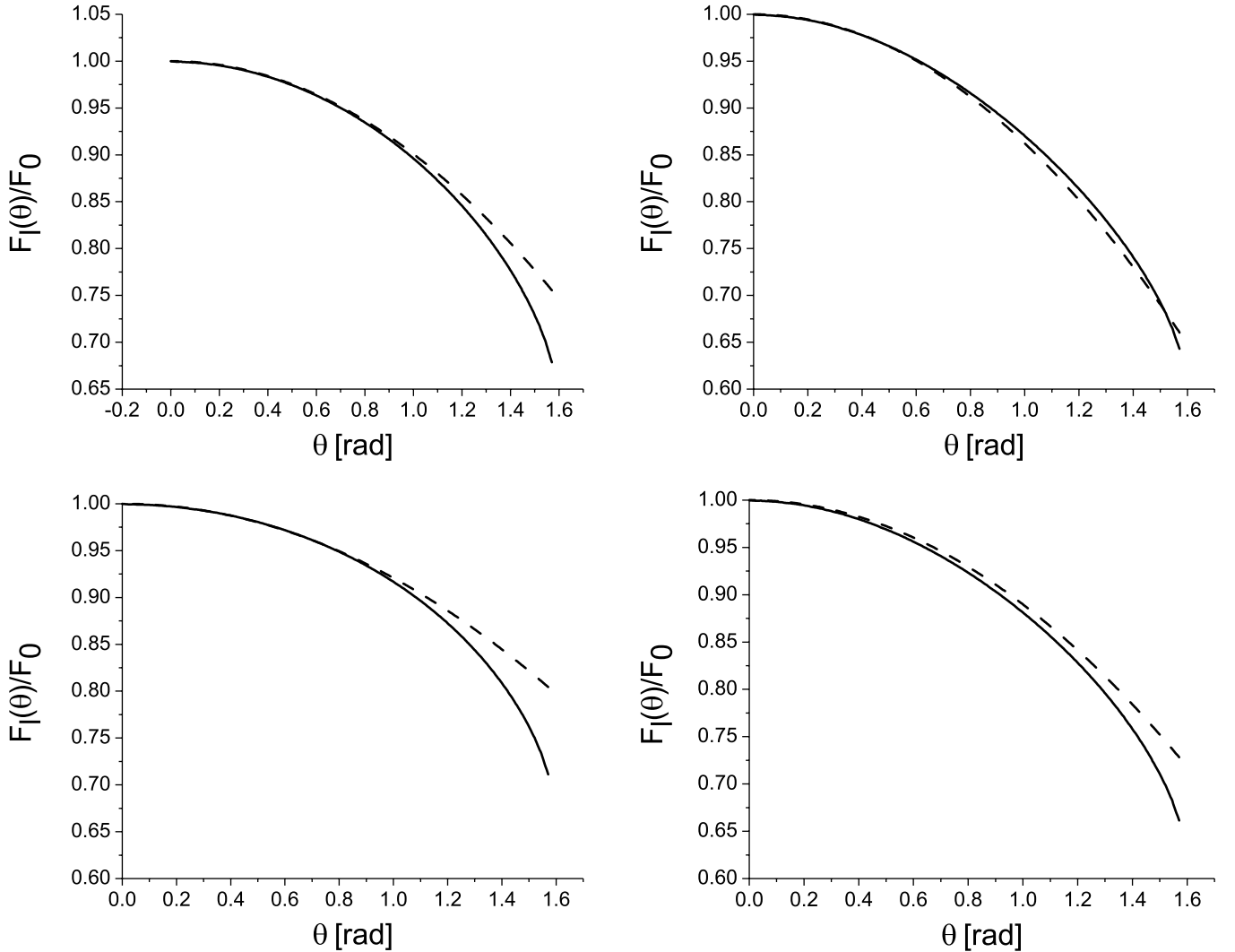


Fig. 4. Local field as a function of the angle  $\theta$  in radians. The full line is extracted data from the solution of the Laplace equation while the dashed line corresponds to Eqs. (12) and (13). The two upper figures corresponds to  $L/R = 30$  with  $D/L = 10$  (left) and  $D/L = 0.1$  (right). Lower figures are for the conditions  $L/R = 300$  with  $D/L = 10$  (left) and  $D/L = 0.01$  (right).

integration of Eq. (1) over the hemisphere:

$$I = \int_0^{\pi/2} j(\theta) 2\pi R^2 \sin(\theta) d\theta \propto 2\pi R^2 \int_0^{\pi/2} \sin(\theta) F_l(\theta)^2 \exp\left(-\frac{4\kappa\phi^{3/2}}{3qF_l(\theta)}\right) d\theta. \quad (14)$$

For a simple operational approximation of this integral, we will ignore the angular dependence in the factor  $F_l(\theta)$  in the pre-exponential and expand the sine function and the argument in the exponential to leading order. If  $4\kappa\phi^{3/2}/3qF_l(\theta = 0)$  is sufficiently large, i.e., for not very high fields, the integration limit can be replaced with infinity and

the integral performed to give

$$I \propto 2\pi R^2 F_l(0)^2 \left(2 \cdot \frac{4\kappa\phi^{3/2}}{3qF_l(0)}\right)^{-1} \times \exp\left(-\frac{4\kappa\phi^{3/2}}{3qF_l(0)}\right). \quad (15)$$

If we factor out the current density at the tip of the electrode, we get the effective area for small emission currents:

$$S_{\text{eff}} = \frac{I}{j(\theta = 0)} = 2\pi R^2 \cdot \frac{3qF_l(0)}{8\kappa\phi^{3/2}}. \quad (16)$$

Fields are small in this connection when they are smaller than the field,  $F_l(0)_c$ , that renders the

correction term to  $2\pi R^2$  in Eq. (16) to unity, i.e., small relative to the field

$$F_l(0)_c = \frac{8\kappa\phi^{3/2}}{3q}. \quad (17)$$

For  $\phi = 2, 5,$  and  $10$  eV, this critical field is  $3.9 \cdot 10^{10}$ ,  $1.5 \cdot 10^{11}$  and  $4.3 \cdot 10^{11}$  V/m, respectively.

The effective area will modify the original Fowler–Nordheim equation which will now include an additional power of the field in the pre-exponential factor:

$$I = S_{\text{eff}} \cdot j = \frac{3R^2 q^4}{16\pi\sqrt{2m}} \frac{\sqrt{\mu}}{(\phi + \mu)\phi^2} \cdot F_l^3 \exp\left(-\frac{8\pi\sqrt{2m}\phi^{3/2}}{3hqF_l}\right), \quad (18)$$

where the local field can be determined with Eqs. (2) and (11).

## 5. Summary

Using numerical solutions of the electrostatic problem, we have calculated the field enhancement factor  $\gamma$  for a cylindrical, end-capped conducting protrusion in a plane capacitor geometry for different protrusion lengths and plate separations, and fitted the numerical data with simple functional forms. A comparison between the existing models in the literature and our model indicates that the results derived here give a better agreement with the values extracted from solving the Laplace equation for small electrode separations. In addition, we have evaluated the angular variation of the local field along the hemispherical end-cap and found that this also depends on the separation between the emitter and the anode. Our main results are given in Eqs. (10), (11), (13) and (18).

## Acknowledgments

This work was financially supported by VR and the Swedish Foundation for Strategic Research (SSF) within the ‘‘CMOS integrated carbon-based nanoelectromechanical systems’’ and EC FP6 funding (contract no. FP6-2004-IST-003673, CANEL). This publication reflects the views of the authors and not necessarily those of the EC. The Community is not liable for any use that may be made of the information contained herein.

## References

1. R. H. Fowler and L. Nordheim, *Proc. R. Soc. Ser. A* **119**, 173 (1928).
2. G. N. Fursey, *Field Emission in Vacuum Microelectronics* (Kluwer Academic/Plenum Publishers, Cop., New York, 2005).
3. J. D. Jackson, *Classical Electrodynamics* (John Wiley and Sons, Inc., New York, 1999).
4. H. C. Miller, *J. Appl. Phys.* **38**, 4501 (1967).
5. Z. Xu, X. D. Bai and E. G. Wang, *Appl. Phys. Lett.* **88**, 133107 (2006).
6. R. C. Smith, D. C. Cox and S. R. P. Silva, *Appl. Phys. Lett.* **87**, 103112/1 (2005).
7. S. Axelsson, E. E. B. Campbell, L. M. Jonsson, J. M. Kinaret, S. W. Lee, Y. W. Park and M. Sveningsson, *New J. Phys.* **7**, 245 (2005).
8. C. J. Edgcombe and U. Valdre, *J. Microscopy* **203**, 188 (2001).
9. R. G. Forbes, C. J. Edgcombe and U. Valdre, *Ultramicroscopy* **95**, 57 (2003).
10. J.-M. Bonard, K. A. Dean, B. F. Coll and C. Klinker, *Phys. Rev. Lett.* **89**, 197602/1 (2002).
11. C. J. Edgcombe and U. Valdre, *Solid-State Electronics* **45**, 857 (2001).
12. G. C. Kokkorakis, A. Modinos and J. P. Xanthakis, *J. Appl. Phys.* **91**, 4580 (2002).
13. X. Q. Wang, M. Wang, P. M. He, Y. B. Xu and Z. H. Li, *J. Appl. Phys.* **96**, 6752 (2004).
14. R. C. Smith, J. D. Carey, R. D. Forrest and S. R. P. Silva, *J. Vac. Sci. Technol. B* **23**, 632 (2005).
15. Y. Saito, K. Hamaguchi, R. Mizushima, S. Uemura, T. Nagasako, J. Yotani and T. Shimojo, *Appl. Surf. Sci.* **146**, 305 (1999).
16. J.-M. Bonard, M. Croci, F. Conus, T. Stoeckli and A. Chatelain, *Appl. Phys. Lett.* **81**, 2836 (2002).
17. I.-M. Choi and S.-Y. Woo, *Appl. Phys. Lett.* **87**, 173104/1 (2005).
18. C. Dong and G. R. Myneni, *Appl. Phys. Lett.* **84**, 5443 (2004).
19. G. Z. Yue, Q. Qiu, B. Gao, Y. Cheng, J. Zhang, H. Shimoda, S. Chang, J. P. Lu and O. Zhou, *Appl. Phys. Lett.* **81**, 355 (2002).
20. D.-S. Chung, S. H. Park, H. W. Lee, J. H. Choi, S. N. Cha, J. W. Kim, J. E. Jang, K. W. Min, S. H. Cho, M. J. Yoon, J. S. Lee, C. K. Lee, J. H. Yoo, J.-M. Kim, J. E. Jung, Y. W. Jin, Y. J. Park and J. B. You, *Appl. Phys. Lett.* **80**, 4045 (2002).
21. C. J. Edgcombe, *Ultramicroscopy* **95**, 49 (2003).
22. FlexPDE<sup>TM</sup>, PDE Solutions, Inc., Finite Element Software (2006), <http://www.pdesolutions.com>.
23. J. H. Jeans, *The Mathematical Theory of Electricity and Magnetism*, 4th edn. (Cambridge University Press, Cambridge, 1920).